npj | climate and atmospheric science

Article

Published in partnership with CECCR at King Abdulaziz University

https://doi.org/10.1038/s41612-024-00654-w

Escalating tropical cyclone precipitation extremes and landslide hazards in South China under Global Warming

Xiaoming Shi[1,2], Yang Liu[3], Jianan Chen[1], Haoming Chen[1], Yueya Wang[1], Zhongming Lu[1], Ruo-Qian Wang[4], Jimmy C.-H. Fung[1,5] & Charles W. W. Ng[3]

Tropical cyclones (TCs) are expected to produce more intense precipitation under global warming. However, substantial uncertainties exist in the projection of coarse-resolution global climate models. Here, we use deep learning to aid targeted cloud-resolving simulations of extreme TCs. Contrary to the Clausius-Clapeyron (CC) scaling, which indicates a 7% moisture increase per K warming, our simulations reveal more complex responses of TC rainfall. TCs will not intensify via strengthened updrafts but through the expansion of deep convective cores with suppression of shallow cumulus and congestus. Consequently, while localized hourly rainfall may adhere to the CC scaling, precipitation accumulation over city-sized areas could surge by 18%K^{-1}. This super-CC intensification due to changing TC structure has profound implications for floods and landslides. Estimations using Hong Kong's slope data confirm this concern and suggest an up to 215% increase in landslide risks with 4-K warming, highlighting amplified threats from compound disasters under climate change.

Climate change will likely cause more frequent and intense extreme weather that can inflict substantial socioeconomic and human losses. We face the pressing task of adapting our infrastructure and risk management strategies to build communities resilient to climate hazards. However, the extent of precipitation changes, particularly in tropical regions, is uncertain due to the variability of extreme rainfall responses to warming in global climate models (GCMs). Tropical cyclone (TC) research[1] suggests a probable increase of TC precipitation by 7.0% per K of global mean temperature rise. Still, this value is shadowed by disparities between GCMs, which display an uncertainty range from 1.5%K^{-1} to 11%K^{-1}. Despite their outliers status, some high-resolution (~25 km) global models[2] suggest an even higher sensitivity of 13–17%K^{-1}. In stark contrast, observation-based studies[3,4] hint at a diminishing trend in the inner-core TC precipitation despite increases in outer rainband precipitation observed.

The challenge in predicting TC precipitation's sensitivity to warming arises from the fundamental scale characteristics of convective weather systems. Despite the organized convection produced in mature TC eyewalls, they are characterized by a combination of slantwise convective clouds with sporadically superimposed buoyant convective cells, while distant rainbands embody primarily organized ordinary deep convection, mostly unconstrained by the TCs' inner-core[5]. A grid resolution of roughly one kilometer is needed to capture these convective cloud dynamics in detail. Such high-resolution global simulations exist[6,7], but their computational demands limit their widespread adoption in long-term climate simulations, leaving the mechanisms behind TC precipitation changes veiled.

Yet, to establish climate-resilient cities and communities, high-resolution forecasting of TC extreme precipitation under global warming is vital. The possible intensification of precipitation influences flood and landslide risks[8–11]. The delicate interplay of fine-scale processes within the climate system[12–15] determines these risks. Unfortunately, comprehensive assessments[16,17] are scarce due to high-resolution climate simulation deficiencies and uncertainties in process models, including hydro-mechanical slope stability models[18].

In this study, we harness the potential of deep learning (DL) to enhance selective dynamical downscaling[19]. Using a DL model, we analyze coarse-resolution global climate simulation data, pinpointing time slices that might foster local extreme precipitation events. These identified large-scale circulation patterns are then applied to drive the Weather Research and Forecast (WRF) model[20] to simulate local events at a 1-km resolution, effectively capturing the intricacies of convective weather dynamics. Our DL-aided selection method yielded more accurate results than the direct selection using GCM rainfall outputs, which, nonetheless, were used

[1]Division of Environment and Sustainability, Hong Kong University of Science and Technology, Hong Kong, China. [2]Center for Ocean Research in Hong Kong and Macau, Hong Kong University of Science and Technology, Hong Kong, China. [3]Department of Civil and Environmental Engineering, Hong Kong University of Science and Technology, Hong Kong, China. [4]Department of Civil and Environmental Engineering, Rutgers, The State University of New Jersey, Piscataway, NJ, USA. [5]Department of Mathematics, Hong Kong University of Science and Technology, Hong Kong, China. e-mail: cecwwng@ust.hk

supplementally to ensure the robustness of our data (see Methods). Our study centers on the South China region (Supplementary Fig. 1), where all extreme cases identified are TCs. A similar targeted modeling strategy has been successful in a previous study assessing the changes in atmospheric river-caused precipitation in California[21]. Our high-resolution simulations unveil significant alterations in TC structures and corresponding rainfall, a finding unachievable with coarse-resolution GCMs. Furthermore, we apply the high-resolution precipitation information to estimate impacts on Hong Kong's slope safety, where about 300 failures occur annually on average.

Results

Super-Clausius–Clapeyron sensitivity of precipitation extremes

Assuming constant relative humidity, the atmospheric moisture amplifies by 7%K^{-1} with global warming. This rate is established by the Clausius-Clapeyron (CC) equation and is thus referred to as CC scaling. Even with constant vertical motions, precipitation sensitivity to warming diverges from the CC rate as the formation of hydrometeors within clouds follows a different temperature dependency than moisture[22]. Despite this, the CC scaling is frequently used as a reference gauge of precipitation sensitivity to warming.

In our study, the GCM simulation of the period 2015 to 2100 under the SSP5-8.5 scenario using the Community Earth System Model 2 (CESM2)[23] at ~100 km resolution demonstrates a sensitivity of 13%K^{-1} in the South China region's daily precipitation extremes. This sensitivity is obtained by linearly regressing CESM2's maximum daily precipitation from each decade to the decadal mean global mean temperature (Supplementary Fig. 2). This translates into a 52% increase in maximum daily precipitation with a 4 K warming when comparing the first and last 20 years of the CESM2 simulation (termed 'present' and 'future' periods for 2015−2034 and 2081−2100, respectively). Applying the DL model directly generates a daily maximum rainfall series for South China (Fig. 1a). The purpose of this estimation by the DL model is to provide a first guess of finer-resolution distribution of rainfall so that our high-resolution WRF downscaling later can target extreme events only. This series reflects the region's seasonal rainfall cycles and an escalating daily maximum over time. The increasing trend is not linear. The third most intense events in some years of the last decade exhibit rainfall higher than that of the strongest events in most years earlier than 2070 (Fig. 1b). Nevertheless, the DL model's predicted rain rate is modest compared to observations, such as the Hong Kong Observatory (HKO) recording a peak daily rainfall of 330 mm after 2000[24]. The lower DL prediction stems from the DL model's training rainfall data[25], which interpolated from station data to 0.25° × 0.25° grid cells. Regardless, the DL model predicts maximum daily rain of 202 and 342 mm for the present and future periods, indicating a climate sensitivity of 17%K^{-1}. Linear regression of DL-predicted decadal rainfall extreme in the South China region (red circles in Fig. 1a) as a function of decadal global mean temperature suggests it has a statistically significant (95% confidence level) temperature dependence of 14%K^{-1}; Regression between annual global mean temperature and annual rainfall extremes does not suggest a statistically significant linear relationship, probably due to strong natural interannual variability (Supplementary Fig. 3). However, it should be noted that the results directly from the DL model are a preliminary estimation only and the use of kilometer-scale resolution simulations below yield a more reliable estimation.

We selected the top 16 events from each 20-year period for further evaluation. They correspond to the top 2.5% of rain events in the South China region. High-resolution WRF simulations of selected events reveal nuanced details of these extreme occurrences. In hindsight, we found that all events crossed the wind threshold for TCs (Supplementary Fig. 4 shows example synoptic conditions for six cases). During the present period, 6 of 16 events reach typhoon intensity or above, including two super typhoons. Conversely, 9 of 16 future extreme events are categorized as typhoons, with three classified as super typhoons. Because our selection criterion is precipitation, assuming all TCs will intensify in a warming world might be inaccurate. Yet, the result suggests that the amplification of extreme precipitation in a warming South China region correlates with TC strengthening and an apparent frequency increase in the most intense ones.

Precipitation extremes in the WRF simulations and their sensitivity to warming, illustrated in Fig. 2, are displayed as functions of spatial and temporal accumulation scales. Running windows of different sizes in space and time were applied to obtain the rain rate at given spatial and temporal

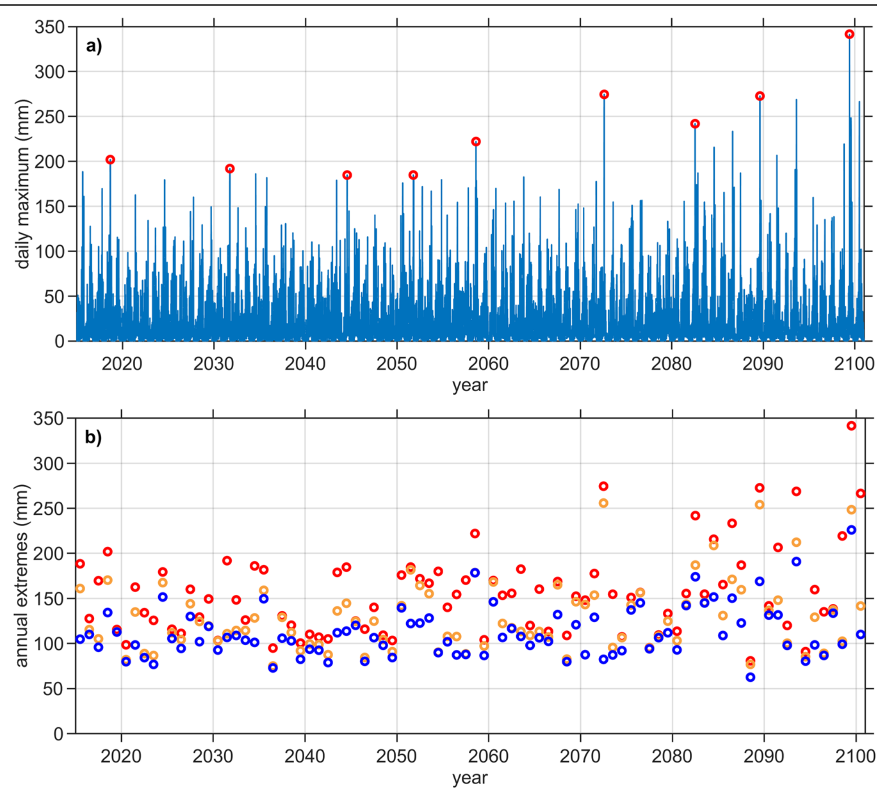

Fig. 1 | The deep-learning model predicted precipitation extremes. a Time series of maximum daily rainfall in the South China region predicted by the trained deep-learning model between 2015 and 2100. The maximum value of each day is the maximum grid-point daily rainfall selected from all 0.25° × 0.25° grid cells in the South China region. Red circles indicate the maximum for each ten-year period starting from 2015. **b** The top three daily rainfall maxima of each year predicted by the deep learning model for 2015−2100. Red circles are the most intense event each year, orange the second, and blue the third.

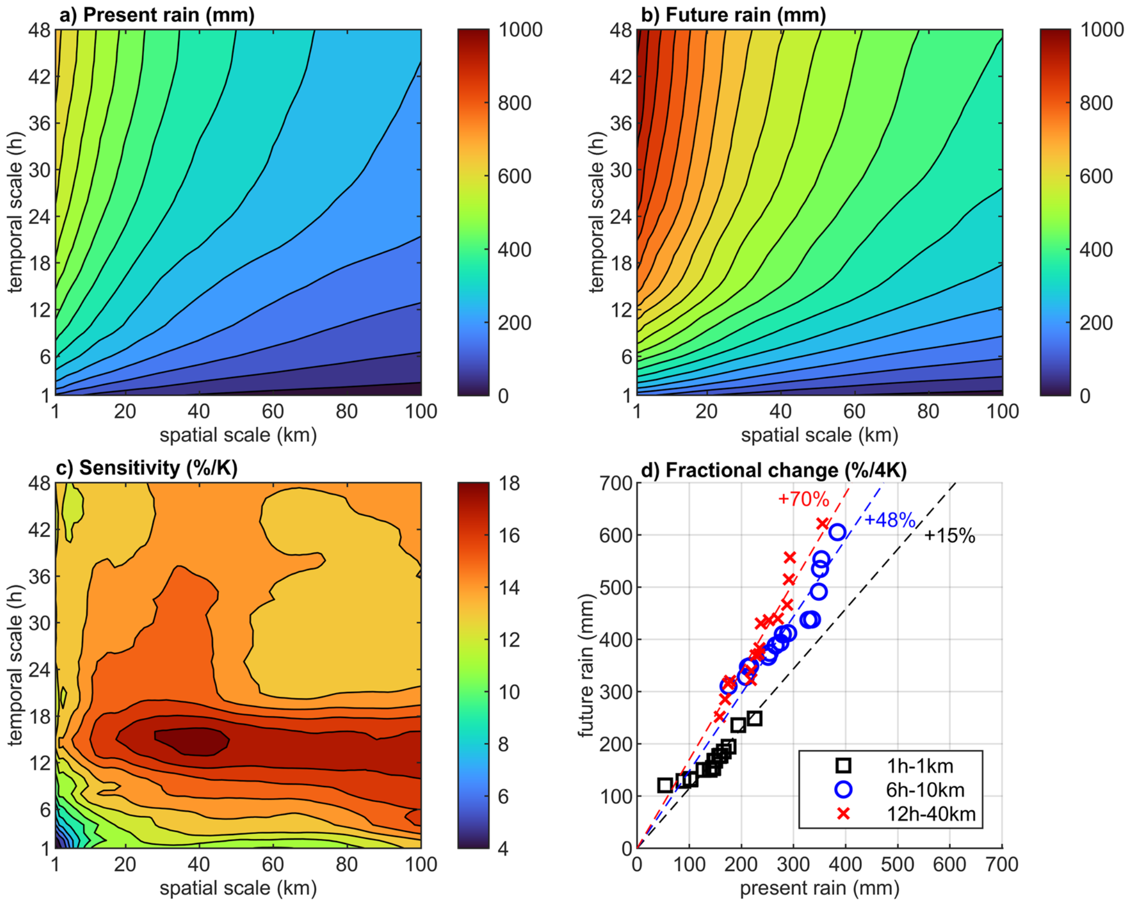

Fig. 2 | The intensity and sensitivity to warming of extreme precipitation as functions of spatial and temporal scales. a The present climate (2015−2034), top 16 event-mean maximum rainfall accumulated over given temporal scales and averaged over square regions of given spatial scales. **b** Same as (**a**), but for future (2081−2100) top 16 events. **c** The sensitivity of extreme rainfall to warming as a function of spatial and temporal scales. **d** Scatter plot comparing the rainfall of the present and future top 16 events for three specific temporal-spatial scales; those cases are re-ranked and then paired for the plot. The percentage values marked near the lines are the results of linear regression.

scales, and the maximum value in space and time from each event was used in the analysis of Fig. 2. Figure 2a, b shows that maximum precipitation accumulates quickly as we extend the time scale, and its spatial average diminishes as we increase the spatial scales of interest. Countering prior studies[26,27] suggesting short-duration extreme rainfall could exhibit super-CC scaling, our results in Fig. 2c indicate precipitation extremes at hourly and kilometer scales show a sensitivity nearing the CC rate, between 4 and 8%K^{-1}. However, when evaluating rainfall accumulation over extended time scales and larger spatial scales, the sensitivity generally trends super-CC. The peak sensitivity is around 18%K^{-1} for the time scales of 12−18 h and spatial scales of 25−50 km. Figure 2d shows that with a 4-K warming, total rainfall escalates by approximately 70% for a 12-h and 40-km scale accumulation, while the increase for 1-hour and 1-km accumulation is only about 15%. Notably, the maximum hourly rainfall in the most intense present-period event was 225 mm, akin to China's highest recorded 202 mm during the 2021 Zhengzhou flooding[28,29]. 24-h accumulated rainfall in the simulations is also close to the observation record (see Methods). This reaffirms that our high-resolution simulations yield reasonable intensities for these extreme events.

Our findings imply that adapting to global warming demands meticulous contemplation of its potential sector-specific impacts. While short-duration rainfall extremes exhibit low sensitivity, the accumulated rain over half-day timescales or more and the spatial scale of typical city sizes are distinctly super-CC. This accelerated intensification poses challenges to urban drainage systems, flood management, and landslide risks.

Scale-dependent sensitivity: storm organization changes

To reconcile our estimation with previous results, we examined the characteristics of convective updraft cores as functions of height for the present period and future extreme events (Fig. 3). Somewhat unexpectedly, the average upward velocity in these cores shows a decrease in the lower and mid-troposphere in future cases (Fig. 3a). Boundary layer top and upper troposphere exhibit some increases in the median values, but the maxima at those levels exhibit decreases as well, with approximately 3 m s^{-1} decrease at upper levels. This dampening of updrafts, which partially cancels out the positive effect of increasing moisture, potentially elucidates why short-duration, small-scale rainfall extremes adhere to a sensitivity close to or lower than the CC rate. Concurrently, the updraft cores within the weather system increase in size for both their median and maximum values (Fig. 3b). The proximity of convective cores to the center of the convection cluster (referring to the collection of convective cores), which is not necessarily the TC center, exhibits no significant change in the lower levels but has significant increases at upper levels in the warmed climate (Fig. 3c). The counts of updraft cores exhibit significant decreases at lower levels but no significant change at upper levels (Supplementary Fig. 5). These alterations suggest deep convective cores in TC rainbands expand horizontally under global warming, and at low levels, shallow cumulus and cumulus congestus are either killed or merged into deep convection due to the expansion. Consequently, even as individual cores weaken slightly in the mid-troposphere with warming, the consolidation of larger cores enhances the spatial and temporal accumulation along the weather system's path to strengthen at a rate exceeding that of small-scale local rainfall.

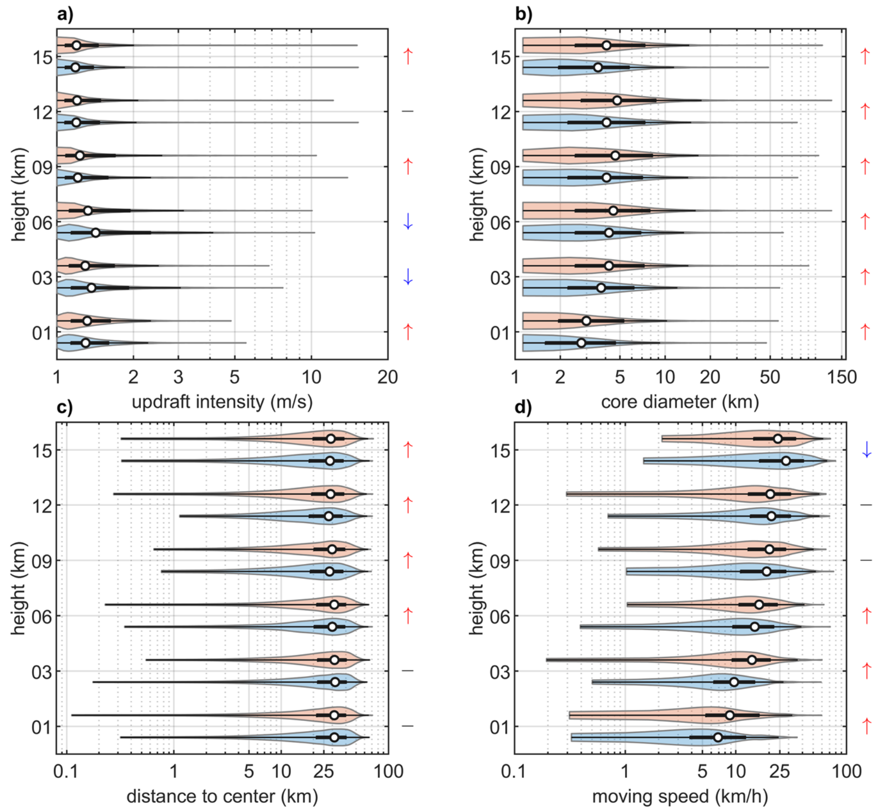

Fig. 3 | The distribution of the characteristics of convective updraft cores in extreme events. a The distribution of updraft intensity, which is the mean velocity in the updraft cores. **b** The distribution of diameters of updraft cores at different height levels. **c** The distribution of the distance between updraft cores and the averaged center of the core cluster. **d** The distribution of core cluster center horizontal moving speed. For each height, the upper orange violins indicate the distribution for future extreme events, and the lower blue violins are for present extreme events. Updraft cores are defined as a two-dimensional continuous region with updraft velocity greater than 1 m s^{-1} everywhere within it. Hourly data for the 24 h producing the maximum rainfall in each case are sampled. The analysis includes all cores within a 100 km radius from the grid point with the maximum 24-h precipitation, which must be within the 1-km domain, but the vertical velocity data is from the larger 3-km resolution domain. The upward arrow (↑), downward arrow (↓), and dash (–) indicate future median values at the corresponding levels increase, decrease, or have no change, respectively, at the 5% significance level according to the Mann−Whitney U-test.

The spatial scales of 25−50 km and temporal scales of 12−18 h exhibit higher sensitivity than other scales, probably because of the characteristic scales of convection clusters and TC rainbands. Spectrum analysis of mid-level vertical velocity around the center of the maximum precipitation (Supplementary Fig. 6a) suggests that the kinetic energy in vertical motions has no change at very small and large scales but exhibits a significant increase at scales roughly between 10 and 100 km. Radially averaged precipitation distribution (Supplementary Fig. 6b) suggests that the *e*-folding radius from the maximum precipitation center is 15 km and 22 km for the present and future cases, respectively. Therefore, the effects of expanding deep convection cores are more prominent at those scales than at the smaller scales of 1−10 km. Meanwhile, the temporal accumulation of rainfall depends on the evolution and movement of rainbands, which include not only convective regions but also stratiform regions. Outgoing longwave radiation (OLR) composite (Supplementary Fig. 6c, d) suggests that the inner area of TC rainbands with strengthened OLR[30] (≤150 Wm^{-2}) is on the scale of 100−200 km. Given that the convective region moves at the speed of about 10−20 m s^{-1} (Fig. 3d), it is reasonable that the time scale of 10−20 h is the duration with significant local rainfall enhancement in TCs. This finding differs from previous studies probably because previous kilometer-scale resolution simulations focused on non-TC convection, which is organized at a smaller spatial scale and has a shorter lifetime.

Local accumulation of precipitation depends on rain intensity and the overlapping time of TC rainbands and the interested local area, the latter of which, as pointed out by earlier studies[31], is inversely proportional to TC translation speed. Previous study[31] hinted that a slowdown of TC translation speed could also contribute to TC precipitation strengthening. Our analysis (Fig. 3d), however, shows that TC-related convection clusters seem to move more quickly at low levels but exhibit no significant change in the upper troposphere except near the tropopause, where they move more slowly in the future climate. However, it should noted that the movement of the convection clusters is mostly dominated by the rotation wind environment of TCs instead of their translation speed. We composited the synoptic fields of the extreme events for 700 hPa and 200 hPa levels (Supplementary Fig. 7) and found that, indeed, the low-level geopotential height field suggests future TCs are substantially stronger. However, at the upper level, the present cases composite exhibits weak easterlies around the TCs, while future TC composite has southerlies to their south and easterlies to the north. Such changes in the upper-level environment are probably related to the response of the western North Pacific subtropical high to global warming[32].

Tracking the movement of sea level pressure low centers of those TCs for 24-h windows producing maximum local 24-h precipitation suggests there is about a 24% increase in the TC centers' translation speed. This discrepancy with previous research findings[31] might mainly be due to the fact that our analysis focused on the 24-h period with maximum precipitation when the TCs are close to the coast and relatively small sets of TCs near the South China region, which do not represent the general trend of TCs. Nevertheless, the recent study by ref. 33 suggests that in the Western North Pacific, TCs' translation speed before they reached their maximum intensity actually increased between 1980 and 2018. They attributed this change in translation speed primarily to the enhancement of TC intensity. Tu et al. [34] further found that the TC rain rate is larger for TCs with a faster translation speed due to low-level inflow enhancement and vertical wind shear. Therefore, while the TC translation speed increase in our cases may be specific to the South China coast, it may have contributed to the stronger convection and higher rain rate in future cases.

Previous modeling studies suggested that the strengthening of TCs due to a warmer sea surface temperature would be counterbalanced by the stabilization of the troposphere under warming[35]. Yet, these studies did not account for cloud-radiative feedback, an element underscored by recent research for its pivotal role in enhancing TCs[36–39]. The changes in the convective core size and organization might stem from enhanced cloud-radiative feedback under warming. The potential causes of the changes in TCs' internal convection organization require further investigation, which is beyond the scope of this study. However, it is worth noting that while including many more TC simulations can yield a larger sample size, the DL model prediction results (Supplementary Fig. 3)

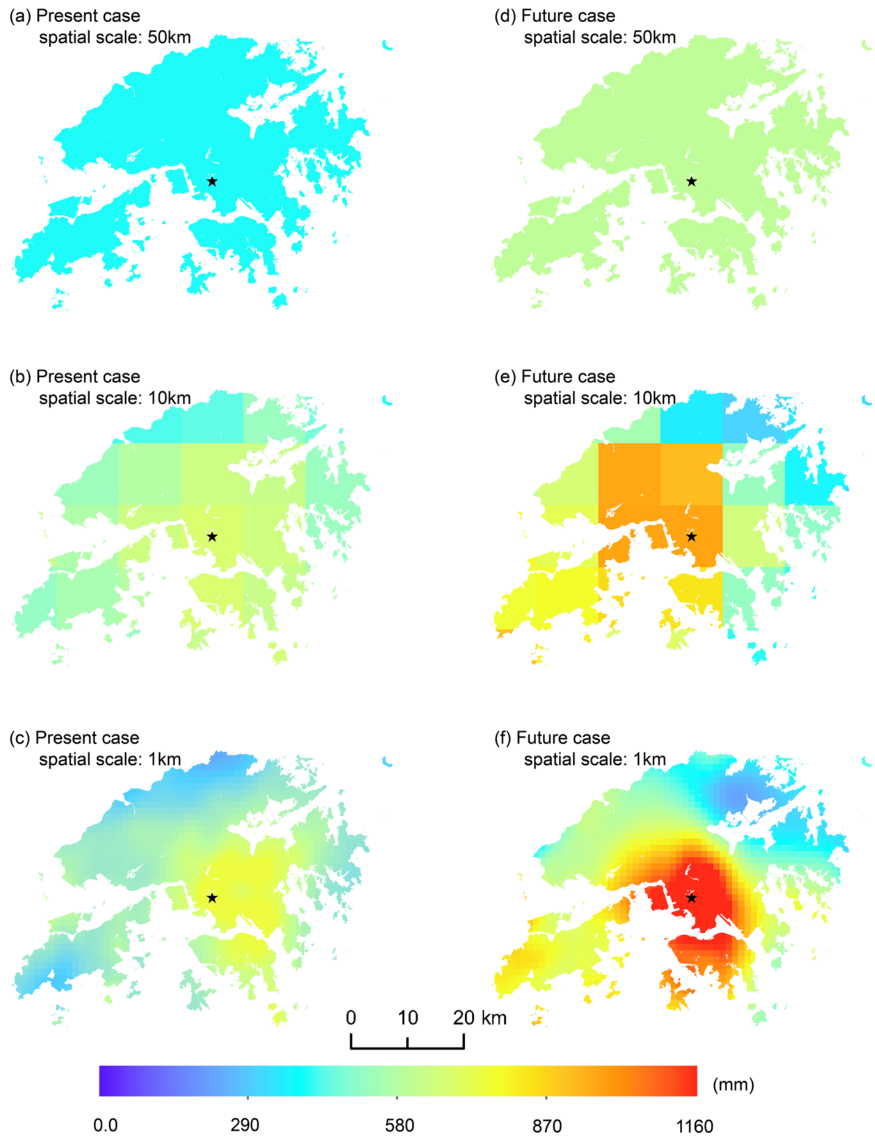

Fig. 4 | Precipitation in the most intense precipitation events in present and future periods. a−c are the spatial distribution of maximum 24-h precipitation of the most intense event in the present period for different spatial averaging scales. **d−f** are for that in the future period. Every grid point searched for its 24-h window in the event independently. The center of precipitation is the point with maximum 24-h rainfall in the event. This center of rain is located at the star symbol for each case. The star symbol represents the shortest total distance from all of Hong Kong's man-made slopes used in this study, also known as the median center. Such a translation enables us to compare the impact of changing precipitation intensity and patterns on the stability of the same slopes.

suggest that a strong correlation might exist only when we examine a small number of extreme events and their corresponding longer-term mean temperature. Nature variability might generate noise that makes the relationship between TC characteristics and short-term temperature statistically insignificant. Future studies need to balance between sample sizes and natural variability.

Impacts from TC structure and intensity changes

The super-CC scaling of extreme precipitation intensity in response to warming, accompanied by changes in spatial-temporal structure, imposes significant implications for climate adaptation. A detailed spatial and temporal distribution of extreme rainfall is vital for assessing its impacts on landslide risks. The 24-h maximum rolling rainfall (MRR) is a commonly adopted metric used by researchers[40,41] to predict landslides that occur on slopes in Hong Kong. Figure 4 shows the 24-h MRR patterns at three different spatial resolutions (50 km, 10 km, and 1 km) for the most intense events in the present and future periods over the Hong Kong region. At 50-km resolution, the 24-h MRR for the most intensive present and future cases are uniform at 399 mm (Fig. 4a) and 602 mm (Fig. 4d), respectively. At 10-km resolution, a 24-h MRR pattern is observed with the rainfall amount ranging from 245 to 684 mm for the present case (Fig. 4b) and 244 to 955 mm for future case (Fig. 4e). At 1-km resolution, the 24-h MRR amount ranges from 209 to 753 mm for the present case (Fig. 4c) and 217 to 1163 mm for the future case (Fig. 4f).

The computed results reveal that the importance of finer spatial resolution is two-fold. Firstly, the spatial details of precipitation predicted at 1 km gradually disappear when the spatial resolution decreases to 10 km and 50 km. Secondly, the maxima of 24-h MRR is reduced for both present and future cases. As a result, the predicted precipitation at the 1-km spatial resolution is around 90% larger than that predicted at the 50-km resolution, which will have severe consequences for estimating the impact of rainfall-induced hazards. Furthermore, comparing the present and future cases at 1-km resolution shows that the maxima of 24-h MRR in future cases increase remarkably by 54% due to 4 K warming. This increase indicates an increase of $13\%K^{-1}$ warming, consistent with the super-CC scaling suggested in Fig. 2c. The CC-scaling ($7\%K^{-1}$) can substantially underestimate the 24-h MRR for future cases.

The number of landslides under given rain events can be predicted based on Hong Kong's Landslip Warning System (LWS)[40], a statistical model based on historical observations. As precipitation in future cases exceeds historical maxima, the LWS is modified to provide a lower-bound prediction of future landslide cases by assuming the number of landslides does not increase when rainfall exceeds the historical maximum. Figure 5 shows the predicted number of landslides against the mean 24-h MRR using

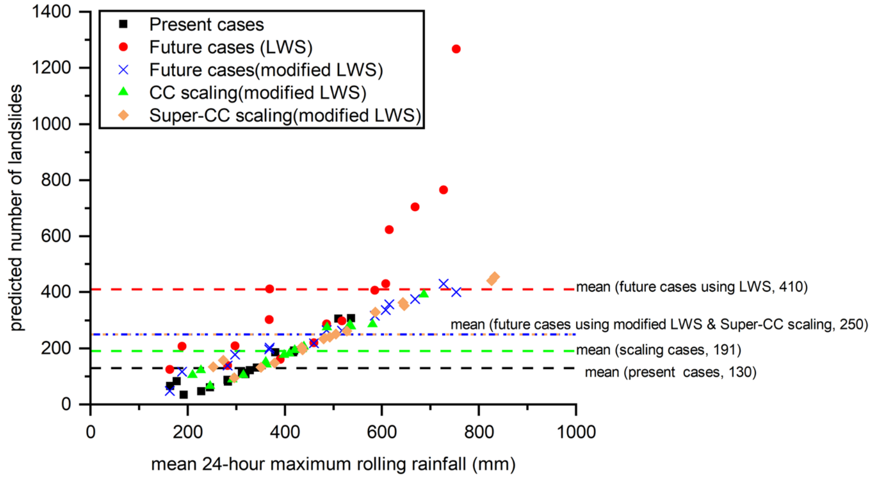

Fig. 5 | Predicted number of landslides for present and future top 16 cases of extreme precipitation. The landslide prediction is based on 24-hour maximum rolling rainfall using Hong Kong's Landslide Warning System (LWS). The mean 24-h maximum rolling rainfall is the average of the maximum 24-h rainfall for each slope in an event. Black squares (■) are the prediction based on the present-period top 16 cases. The red circles (●) are the prediction based on the current LWS and the future-period top 16 case rainfall. The blue crosses (×) are based on a modified LWS, which assumes the number of landslides does not increase when rainfall exceeds the historical maximum (see Methods). The green triangles (▲) and orange diamonds (♦) are the predictions using modified LWS, where the precipitation in the present-period 16 cases are assumed to increase according to CC scaling of 7%K^{-1} and super-CC scaling of 13%K^{-1}, respectively.

the current and modified LWS. For the present cases (black squares), the existing and modified LWS give almost identical predictions for the number of landslides because the precipitation does not exceed the historical maxima for most areas. The average number of predicted landslides for present cases is 130. If we assume the precipitation increases according to CC-scaling (green triangles), which implies an increase of 28% of precipitation for the 4 K warming compared with present cases, the average number of predicted landslides will rise to 191 (+47%) by the end of this century. However, when we use the actual high-resolution simulation data, the average predictions using the modified LWS (blue crosses) and current LWS (red circles) show 250 (+92%) and 410 (+215%) landslides, respectively, for the future extreme cases. For the modified LWS, the increase is more due to the expansion of heavy rain area than the strengthening of rainfall because the landslide risk plateaus when rainfall exceeds the historical maximum. Therefore, future rainfall scenarios with 4 K warming reveal an increase in the number of landslides up to 215% by the end of the century, highlighting amplified threats from landslides under climate change.

It is worth noting that the actual high-resolution simulation data also reveals that the 24 h MRR in extreme events increases by 13%K^{-1} warming as opposed to the CC scaling assumption of 7%K^{-1}, and this sensitivity can be directly used for estimating the change in landslides. The prediction of the number of future landslides from amplifying the present-case 24 h MRR according to the super-CC scaling of 13%K^{-1} and using the modified LWS is shown in orange diamonds in Fig. 5, which indicate an average of 250 landslides (+92%), the same as that predicted for the future cases using the actual rainfall. Using the current LWS and applying the super-CC scaling also yield good approximations, though the expected number of future landslides is not identical to that using actual precipitation data (Supplementary Fig. 8). This exercise implies that our estimation of the scale-dependent sensitivity of extreme precipitation, as shown in Fig. 2c, has some degrees of generalizability and can be used to estimate the responses of precipitation-related hazards to global warming.

Discussion

Determining the response of tropical precipitation extremes to global climate change has been a notoriously difficult task for global climate models[22,42,43]. The inherent uncertainties in these models have often led to substantial variations in their projections. Our study used cloud-resolving simulations to explicitly resolve convection details, providing a more reliable assessment of extreme precipitation response to global warming, specifically for TCs in the South China coastal region.

Contrary to past studies that typically propose a singular sensitivity of precipitation extremes, our evaluation reveals scale-dependent sensitivities. When considering kilometer-scale spatial averages and short-duration accumulation, we found that the sensitivity of extreme precipitation approximates the classic Clausius-Clapeyron (CC) scaling, ~7%K^{-1}. However, when factoring in rainfall accumulation over larger spatial scales (20−50 km) and temporal scales (10−24 h), the sensitivity of accumulated precipitation surpasses the doubled CC scaling rate. These results have important implications: on the scales relevant to managing flood and landslide risks for typical cities, TC-induced extreme precipitation demonstrates an accelerated intensification under global warming.

Our analysis suggests that this super-CC scaling stems from the expansion of convective cores in future TCs despite slightly weakening their upward motions under warming conditions. Analogous findings have been observed using cloud-resolving simulations for mesoscale convective systems (MCSs), which show an accelerated intensification of precipitation averaged over a scale of about 40 km due to the enhancement and changed organization of convective cores[44,45].

Using kilometer-scale resolution is critical for faithfully assessing the impact of extreme precipitation. We employed a statistical model to estimate the landslide risks in Hong Kong from such extreme events. Global warming can potentially amplify the number of landslides by 92 to 215%. The structural modifications in extreme precipitation are decisive in governing how landslides respond to warming. Owing to the nonlinear relationship between rainfall and landslides, landslide risks may escalate severalfold relative to precipitation intensification. Global warming has the potential to unleash amplified societal repercussions via compound events[46–48]. For instance, Hurricane Harvey in 2017 delivered catastrophic rainfall in and around Houston, and its effects were exacerbated by a slow-moving storm surge causing extensive flooding[49]. Super Typhoon Mangkhut in 2018 is another example, where extensive rainbands, severe winds, and subsequent storm surges culminated in substantial damages in the Philippines and South China[50].

However, while the kilometer-scale resolution simulations represent a significant advancement relative to coarse-resolution GCMs, they are tools with limitations. They still necessitate complex turbulence parameterization — an area at the forefront of model development demanding efforts in the relevant physics[51]. Challenges also reside in the limited distribution of the observation network required for model validation. Weather stations, typically dispersed between 1 and 100 km, are strategically situated in rural areas to mitigate disruptions to human activities and infrastructure[52,53], and weather radars are usually spaced over 100 km apart. Since flash floods and landslides are highly localized phenomena, accurately modeling them remains challenging for both models and observations. Therefore, this study underscores the necessity for high-resolution data, especially in urban regions, to capture the spatial dynamics of extreme rainfall.

The intensification of TCs and subsequent landslides, rising sea levels, and storm surges present formidable challenges for climate change adaptation. These challenges encompass reinvestment in urban drainage infrastructure to prevent flooding, relocation of at-risk communities, and comprehensive climate risk management. To provide the scientific evidence needed for reinventing infrastructure and relocating communities, integrated risk assessments of TCs will be essential. While early warning systems for TCs are well-established, risk management strategies before, during, and after TCs in coastal cities like Hong Kong and many others remain underdeveloped. Climate adaptation for coastal cities threatened by TCs will necessitate increased cross-disciplinary collaboration.

Methods

Selective dynamical downscaling

The deep learning model structure follows the previous work[19]. Its structure features regular convolution and channel-wise separable convolution operations. The model in the last work was designed for classification, but here, we added a regression layer to predict rain intensity. Its training dataset for atmospheric circulation is from the ERA5 reanalysis[54], including five variables (geopotential, specific humidity, temperature, u and v components of wind) at six pressure levels (250, 500, 600, 700, 850, and 925 hPa) for 18 years (1998 to 2015) in 6-h intervals. The ERA5 data is coarsened to 1° latitude by 1° longitude using linear interpolation to match the resolution of the global climate model. The training dataset for precipitation, the model prediction target, is APHRODITE's (Asian Precipitation - Highly-Resolved Observational Data Integration Towards Evaluation) gridded daily precipitation[25] for 1998−2015. The precipitation data has a spatial resolution of 0.25° latitude by 0.25° longitude. We group precipitation data onto 4×4 blocks so that each block corresponds to one atmospheric circulation data grid cell. Then, we record the maximum daily rainfall among the 4×4 grid cells of each block and use it as the training target for the deep learning model. To predict the maximum rainfall of each block, the deep learning model takes in the atmospheric circulation data in a $48° \times 48°$ square region centered at the block.

After training, the deep learning model was applied to six-hourly climate simulation data from the Community Earth System Model 2 (CESM2)[23] run under the SSP5-8.5 scenario for 2015−2100. We predicted the daily subgrid maximum rainfall for the South China coastal region (Supplementary Fig. 1 innermost domain). The first and last 20 years of the SSP5-8.5 run were defined as "present" and "future" periods. The top 16 cases for the present (2015−2034) and future (2081−2100) periods were simulated with the Weather Research and Forecast (WRF)[20] model, which used four nested domains and 1 km grid spacing in the innermost domain (Supplementary Fig. 1) and 75 vertical levels up to 10 hPa. Physical parameterizations used in the simulations are listed in Supplementary Table 1. If we define one rain event as a number of consecutive days with minimum daily precipitation larger than 5 mm in at least one grid cell in the South China region, we have approximately 600 to 700 events per 20 years. Therefore, the top 16 events approximately correspond to the top 2.5% of all rain events. The simulation of each event was run for a few days, with at least one day before the day of the DL model-predicted rain maximum and one day after. If the DL model selected two or more consecutive days, they were merged and treated as one event.

The above deep learning-assisted approach is named smart dynamical downscaling (SDD). Another possible method for selecting extreme cases is examining the precipitation from CESM2 directly, and it can be referred to as direct dynamical downscaling (DDD). The drawback is that we can only get a coarse resolution ($1° \times 1°$) rainfall, which is not necessarily proportional to smaller-scale rain intensity. Nonetheless, it is helpful to test this approach and supplement the set of extreme events from SDD. Therefore, we also selected the top 16 extreme cases for the present and future periods by examining the CESM2 precipitation outputs and conducting WRF simulations. The SDD and DDD selections have some overlap. For the present period, seven cases appear on both the SDD and DDD top 16 lists, and for the future period, six cases appear on both lists. Therefore, the total number of WRF simulations we ran for the present and future periods, combining SDD and DDD recommendations, are 25 and 26 cases. We rerank those cases based on their WRF daily precipitation coarsened to a 25-km resolution grid mesh. Supplementary Fig. 9 shows that the SDD selections are more accurate recommendations, especially for the future. Precision@k in the figure measures the proportion of relevant recommended items in a recommendation list of size k. For example, for $k = 8$ and the future period, SDD's precision is 5/8, and DDD's precision is 1/4. That means five out of SDD's top eight recommendations appeared in the final top eight list, while only two out of DDD's top eight list. One of the final eight cases was neither in SDD's nor DDD's top eight list. Nonetheless, we dropped the weaker precipitation cases and kept the top 16 cases in the combined present and future sets for further analysis.

It is worth noting that the high-resolution WRF simulations can generate precipitation extremes comparable to observation. The observed maximum 24-h rainfall in Guangdong Province between 2003 and 2017 is 707.6 mm, recorded on September 21, 2010[55]. Hong Kong's maximum 24-h rainfall after 2000 is 638.5 mm, which was recorded on September 8, 2023[56]. Those two cases were related to decaying Typhoons Fanapi and Haikui, respectively. From our WRF simulations for the period of 2015−2023, the top 3 cases of maximum 24-h (grid-point scale) rainfall have values of 707.7, 609.6, and 594.3 mm.

Regional landslide prediction

Hong Kong has a well-documented landslide inventory and currently applies a LWS based on this inventory[40]. Due to urban development, approximately 60,000 man-made slopes are densely distributed across the land area of Hong Kong (Supplementary Fig. 10). The total number of landslides that happened on these man-made slopes under a rain event can be predicted by summing the probability of landslides on each slope when the 24-h rolling rainfall is obtained. To enable the prediction of landslides under extreme rain in the future, the rainfall pattern is shifted from the point with the maximal 24-h rolling rainfall to the median center of Hong Kong's man-made slopes. Moreover, the landslide conditioning factors associated with the man-made slopes such as material properties, slope geometries, maintenance conditions[41,57], are assumed constant. Only the rainfall conditions are changed, which is explicitly carried out to isolate the impact of rainfall on landslides and quantify the effects of future extreme rainfall on landslides.

The bi-linear relationship between the logarithm of landslide frequency and precipitation in the current LWS is based on historical rainfall records and landslide inventory (black lines in Supplementary Fig. 11). However, it is questionable to apply the current LWS to predict the number of landslides for future cases, as the precipitation for future cases exceeds the range of the historical data of the LWS. To address this issue, we provide a modified version of the LWS, in which the rainfall that exceeds the range of historical data (800 mm for soil-cut slopes and 600 mm for rock-cut slopes, fill slopes, and retaining walls) does not cause the landslide frequency increases (red dash lines in Supplementary Fig. 11). This might be over-optimistic. However, during intense rainfalls, surficial permeability governs infiltration; thus, some rainwater becomes surface runoff when rainfall intensity far exceeds the surficial permeability. This implies that a storm with higher intensity does not necessarily produce a more adverse effect on slope stability once a critical return period is reached because infiltration depends on surficial permeability[58]. Therefore, the modified LWS offers a lower bound for estimating future extreme precipitation-induced landslides.

Data availability

The ERA5 reanalysis data is available in the Copernicus Climate Change Service's (C3S) Climate Data Store (https://cds.climate.copernicus.eu/). The APHRODITE precipitation data is available on its project website (http://aphrodite.st.hirosaki-u.ac.jp/). The CESM2 simulation data was downloaded from the Coupled Model Intercomparison Project Phase 6 (CMIP6) website (https://pcmdi.llnl.gov/CMIP6/). Our WRF simulations include a large volume of data, which are available upon request.

Code availability

The codes used to preprocess data, train and apply the deep learning model, and prepare WRF simulations are available at https://github.com/MetLab-HKUST/SDD.

Received: 29 September 2023; Accepted: 18 April 2024;
Published online: 21 May 2024

References

1. Knutson, T. et al. Tropical cyclones and climate change assessment: Part II: projected response to anthropogenic warming. *Bull. Am. Meteorol. Soc.* **101**, E303 (2020).
2. Liu, M. et al. Causes of large projected increases in hurricane precipitation rates with global warming. *npj Clim. Atmos. Sci.* **2**, 38 (2019).
3. Tu, S. et al. Recent global decrease in the inner-core rain rate of tropical cyclones. *Nat. Commun.* **12**, 1948 (2021).
4. Guzman, O. & Jiang, H. Global increase in tropical cyclone rain rate. *Nat. Commun.* **12**, 5344 (2021).
5. Houze, R. A. Jr. Clouds in tropical cyclones. *Mon. Wea. Rev.* **138**, 293 (2010).
6. Wedi, N. P. et al. A baseline for global weather and climate simulations at 1 Km resolution. *J. Adv. Model. Earth Syst.* **12**, e2020MS002192 (2020).
7. Hohenegger, C. et al. ICON-Sapphire: simulating the components of the earth system and their interactions at kilometer and subkilometer scales. *Geosci. Model Dev.* **16**, 779 (2023).
8. Ozturk, U. et al. How climate change and unplanned urban sprawl bring more landslides. *Nature* **608**, 262 (2022).
9. O'Gorman, P. A. Sensitivity of tropical precipitation extremes to climate change. *Nat. Geosci.* **5**, 697 (2012).
10. Prein, A. F. & Heymsfield, A. J. Increased melting level height impacts surface precipitation phase and intensity. *Nat. Clim. Change* **10**, 771 (2020).
11. Zhang, W. et al. Increasing precipitation variability on daily-to-multiyear time scales in a warmer world. *Sci. Adv.* **7**, eabf8021 (2021).
12. Diffenbaugh, N. S. et al. Fine-scale processes regulate the response of extreme events to global climate change. *Proc. Natl Acad. Sci. USA* **102**, 15774 (2005).
13. Gariano, S. L. & Guzzetti, F. Landslides in a changing climate. *Earth-Sci. Rev.* **162**, 227 (2016).
14. Handwerger, A. L. et al. Landslide sensitivity and response to precipitation changes in wet and dry climates. *Geophys. Res. Lett.* **49**, e2022GL099499 (2022).
15. Patton, A. I. et al. Landslide response to climate change in permafrost regions. *Geomorphology* **340**, 116 (2019).
16. Alvioli, M. et al. Implications of climate change on landslide hazard in Central Italy. *Sci. Total Environ.* **630**, 1528 (2018).
17. Sangelantoni, L. et al. Impact of climate change on landslides frequency: the Esino river basin case study (Central Italy). *Nat. Hazards* **93**, 849 (2018).
18. Melchiorre, C. & Frattini, P. Modelling probability of rainfall-induced shallow landslides in a changing climate, Otta, Central Norway. *Clim. Change* **113**, 413 (2012).
19. Shi, X. Enabling smart dynamical downscaling of extreme precipitation events with machine learning. *Geophys. Res. Lett.* **47**, e2020GL090309 (2020).
20. Skamarock, W. C. et al. A description of the advanced research WRF Model Version 4.3. (No. NCAR/TN-556+STR). https://doi.org/10.5065/1dfh-6p97 (2021).
21. Huang, X. et al. Future precipitation increase from very high resolution ensemble downscaling of extreme atmospheric river storms in California. *Sci. Adv.* **6**, eaba1323 (2020).
22. O'Gorman, P. A. & Schneider, T. The physical basis for increases in precipitation extremes in simulations of 21st-century climate change. *Proc. Natl Acad. Sci. USA* **106**, 14773 (2009).
23. Danabasoglu, G. et al. The Community Earth System Model version 2 (CESM2). *J. Adv. Model. Earth Syst.* **12**, e2019MS001916 (2020).
24. Hong Kong Observatory. Ranking Of Highest Daily Rainfall (1884-2022). https://www.hko.gov.hk/en/cis/statistic/erank.htm (2022).
25. Yatagai, A. et al. APHRODITE: constructing a Long-Term daily gridded precipitation dataset for asia based on a dense network of rain gauges. *Bull. Am. Meteor. Soc.* **93**, 1401 (2012).
26. Westra, S. et al. Future changes to the intensity and frequency of short-duration extreme rainfall. *Rev. Geophys.* **52**, 522 (2014).
27. Fowler, H. J. et al. Anthropogenic intensification of short-duration rainfall extremes. *Nat. Rev. Earth Environ.* **2**, 107 (2021).
28. Zheng, Q. et al. Inundation risk assessment based on G-DEMATEL-AHP and its application to Zhengzhou flooding disaster. *Sustain. Cities Soc.* **86**, 104138 (2022).
29. Nie, Y. & Sun, J. Moisture sources and transport for extreme precipitation over Henan in July 2021. *Geophys. Res. Lett.* **49**, e2021GL097446 (2022).
30. Feng, Z. et al. Top-of-atmosphere radiation budget of convective core/stratiform rain and anvil clouds from deep convective systems. *J. Geophys. Res. Atmos.* **116**, D23202 (2011).
31. Kossin, J. P. A global slowdown of tropical-cyclone translation speed. *Nature* **558**, 104 (2018).
32. Choi, W. & Kim, K. Y. Summertime variability of the western North Pacific subtropical high and its synoptic influences on the East Asian weather. *Sci. Rep.* **9**, 7865 (2019).
33. Gong, D. et al. Trends of tropical cyclone translation speed over the western North Pacific during 1980−2018. *Atmosphere* **13**, 896 (2022).
34. Tu, S. et al. Increase in tropical cyclone rain rate with translation speed. *Nat. Commun.* **13**, 7325 (2022).
35. Kieu, C. & Zhang, D.-L. The control of environmental stratification on the hurricane maximum potential intensity. *Geophys. Res. Lett.* **45**, 6272 (2018).
36. Fovell, R. G. et al. Influence of cloud microphysics and radiation on tropical cyclone structure and motion. *Meteor. Monogr.* **56**, 11.1 (2016).
37. Ruppert, J. H. et al. The critical role of cloud–infrared radiation feedback in tropical cyclone development. *Proc. Natl Acad. Sci. USA* **117**, 27884 (2020).
38. Muller, C. J. & Romps, D. M. Acceleration of tropical cyclogenesis by self-aggregation feedbacks. *Proc. Natl Acad. Sci. USA* **115**, 2930 (2018).
39. Yang, B. et al. Cloud-radiation feedback prevents tropical cyclones from reaching higher intensities. *Geophys. Res. Lett.* **49**, e2022GL100067 (2022).
40. Kong et al. Hong Kong's landslip warning system—40 years of progress. *Landslides* **17**, 1453–1463 (2020).
41. Xiao, T. et al. Predicting spatio-temporal man-made slope failures induced by rainfall in Hong Kong using machine learning techniques. *Géotechnique* **73**, 749 (2023).
42. Donat, M. G. et al. More extreme precipitation in the world's dry and wet regions. *Nat. Clim. Change* **6**, 508 (2016).
43. Bacmeister, J. T. et al. Projected changes in tropical cyclone activity under future warming scenarios using a high-resolution climate model. *Clim. Change* **146**, 547 (2018).
44. Prein, A. F. et al. Increased rainfall volume from future convective storms in the US. *Nat. Clim. Change* **7**, 880 (2017).

45. Dougherty, E. M. et al. Future simulated changes in Central U.S. mesoscale convective system rainfall caused by changes in convective and stratiform structure. *J. Geophys. Res. Atmos.* **128**, e2022JD037537 (2023).
46. Zscheischler, J. et al. Future climate risk from compound events. *Nat. Clim. Change* **8**, 469 (2018).
47. Quesada-Román, A. et al. Relationships between earthquakes, hurricanes, and landslides in Costa Rica. *Landslides* **16**, 1539 (2019).
48. Poschlod, B. et al. Climate change effects on hydrometeorological compound events over southern Norway. *Weather Clim. Extremes* **28**, 100253 (2020).
49. Valle-Levinson et al. Compound flooding in Houston-Galveston Bay during Hurricane Harvey. *Sci. Total Environ.* **747**, 141272 (2020).
50. Hong Kong Observatory. Super Typhoon Mangkhut (1822), Tropical Cyclone Reports and Publications. https://www.hko.gov.hk/en/informtc/mangkhut18/report.htm (2018).
51. Shi, X. et al. Key elements of turbulence closures for simulating deep convection at kilometer-scale resolution. *J. Adv. Model. Earth Syst.* **11**, 818 (2019).
52. Muller, C. L. et al. Toward a standardized metadata protocol for urban meteorological networks. *Bull. Am. Meteor. Soc.* **94**, 1161 (2013).
53. Oke, A. Innovation types and innovation management practices in service companies. *Int. J. Oper. Prod.* **27**, 564 (2007).
54. Hersbach, H. et al. ERA5 hourly data on pressure levels from 1940 to present. Copernicus Clim. Change Serv. (C3S) Climate Data Store (CDS), https://doi.org/10.24381/cds.bd0915c6 (2023).
55. Wu, H. Y., Li, Z. H., Li, W. Y. & Zheng, J. Characteristics analysis of extremely severe precipitation based on regional automatic weather stations in Guangdong. *J. Meteorol. Mon.* **46**, 801 (2020).
56. Hong Kong Observatory. The Weather of September 2023. https://www.hko.gov.hk/en/wxinfo/pastwx/mws2023/mws202309.htm
57. Ng, C. W. W., Yang, B., Liu, Z. Q., Kwan, J. S. H. & Chen, L. Spatiotemporal modelling of rainfall-induced landslides using machine learning. *Landslides* **18**, 2499 (2021).
58. Ng, C. W. W., Wang, B. & Tung, Y.-K. Three-dimensional numerical investigations of groundwater responses in an unsaturated slope subjected to various rainfall patterns. *Can. Geotech. J.* **38**, 1049 (2001).

Acknowledgements

The authors acknowledge the fund support by the Research Grants Council of Hong Kong SAR, China (AoE/E-603/18, T31-603/21-N, and HKUST-16307323) and the Center for Ocean Research in Hong Kong and Macau (CORE), a joint research center between the Laoshan Laboratory and the Hong Kong University of Science and Technology (HKUST). The authors thank HKUST Fok Ying Tung Research Institute and National Supercomputing Center in Guangzhou Nansha sub-center for providing high-performance computational resources.

Author contributions

C.N., J.F. and X.S. were responsible for conceptualization, funding acquisition, and supervision. X.S., Y.L., J.C. and H.C. conducted simulations and initial analysis. X.S., Y.L., Z.L. and R.L. wrote the original draft, and all other authors reviewed and edited the final manuscript.

Competing interests

The authors declare no competing interests.

Additional information

Supplementary information The online version contains supplementary material available at https://doi.org/10.1038/s41612-024-00654-w.

Correspondence and requests for materials should be addressed to Charles W. W. Ng.